EUROfusion

WPPFC-CPR(18) 21151

X Courtois et al.

Full coverage infrared thermography diagnostic for WEST machine protection

Preprint of Paper to be submitted for publication in Proceeding of
30th Symposium on Fusion Technology (SOFT)

This work has been carried out within the framework of the EUROfusion Consortium and has received funding from the Euratom research and training programme 2014-2018 under grant agreement No 633053. The views and opinions expressed herein do not necessarily reflect those of the European Commission.

Full coverage infrared thermography diagnostic for WEST machine protection

X. Courtois[a], MH. Aumeunier[a], C. Balorin[a], JB. Migozzi[b], M. Houry[a], K. Blanckaert[a], Y. Moudden[a], C. Pocheau[a], A. Saille[a], E. Hugot[c], M. Marcos[c], S. Vives[a] and WEST Team[a]
[a] CEA, Institute for Research on Fusion by Magnetic confinement, 13108 Saint-Paul-Lez-Durance, France
[b] JBM Optique, 11 avenue de la division Leclerc, 92310 Sèvres, France
[c]Aix-Marseille Univ, CNRS, CNES, LAM, Marseille, France

xavier.courtois@cea.fr

The WEST platform aims at testing ITER like W divertor targets in an integrated tokamak environment. To operate long plasma discharges, IR thermography is required to monitor the main plasma facing components by means of real time surface temperature measurements, while providing essential data for various physics studies.

To monitor the new divertor targets, the WEST IR thermography protection system has been deeply renewed, to match the new tokamak configuration. It consists of 7 endoscopes located in upper ports viewing the whole lower divertor and the 5 heating devices. Electronic devices and computers allow real time video frames processing at 50 Hz rate, to ensure the protection of the main plasma facing components during plasma discharges by a feedback control of the heating devices injected power, and the data storage of ≈3 Gb/s IR images.

Each endoscope provides 2 views covering 2 divertor sectors of 30° (toroidally) and 1 view of a heating antenna. Each optical line is composed of a tight entrance window followed by a head objective which forms an image transported through the endoscope by a series of 4 optical relays and mirrors, up to a camera objective. Finally, 12 IR cameras specially developed for WEST environment capture the thermographic data, at the wavelength of 3.9 μm, with a 640x512 pixels frame size.

The paper describes the design constraints and diagnostic technologies: optics, mechanics, electronics, hard & software, cameras. The laboratory characterization procedures (Modulation Transfer Function, slit response, calibration), and the measurement performance results are given (spatial resolution, temperature threshold). Finally, first results obtained during experimental campaigns in WEST are presented.

Keywords: Infrared thermography, temperature monitoring, plasma facing component, safe operation

1 Introduction

1.1 Context

There is a compelling need for fusion machine protection to measure the surface temperature of Plasma Facing Components (PFC) in order to ensure their integrity and control plasma discharge injected power. This is the role devoted to infrared (IR) thermography.

Tore Supra (TS) was a Carbon-based limiter machine, operated with L-mode from 1988 to 2012. It has been upgraded to WEST, after 5 years of intensive work. WEST is now a full metallic environment tokamak, with an X-point tungsten divertor device and is capable of H-mode during long pulses [1]. Its ITER like divertor plasma facing units, made of bulk W or W coated graphite can be submitted to heat flux deposition up to 10 MW/m². The first plasma occurred in WEST at the end of 2016.

IR monitoring was routinely done is TS since the '90s, and with a real time processing since 2005. This allowed plasma campaigns with long and high-power discharges for years. For WEST, the IR monitoring remains a priority to operate the machine safely, and to provide essential data for various physics studies addressed by high heat flux deposition on components.

1.2 Infrared thermography diagnostics on WEST

The WEST IR thermography system consists of several different diagnostics which all share the same data processing and acquisition system.

The most important diagnostic, which is the object of this paper, is the result of a full refurbishment of the formers IR endoscopes used on TS. It consists of a set of 12 IR cameras mounted on 7 endoscopes located in the upper ports of the machine and viewing downward. It brings a full coverage of the lower divertor, the baffle leading edge and the 5 heating devices: 3 Ion Cyclotron Resonance Heating (ICRH) antennas and 2 Lower Hybrid Current Drive (LHCD) antennas.

New diagnostics were also developed for WEST: a wide angle tangential view located in an equatorial port, a very high resolution view focused on the divertor with a 0.1 mm spatial resolution, and 2 complementary views of the divertor (direct view through a window) and of a LHCD antenna (tangential view through a fibre bundle).

This paper is focused on the set of 7 upper port endoscopes. The others diagnostics are described in [2].

author's email: xavier.courtois@cea.fr

2 Diagnostic description

2.1 Location and lines of sight

For machine protection, the main diagnostic is the set of 7 upper endoscopes spatially distributed on the machine upper ports to cover the full lower divertor (with some overlap) and the 5 heating devices. In that aim, each endoscope has 3 optical lines enabling 2 divertor views and 1 antenna view (Fig 1).

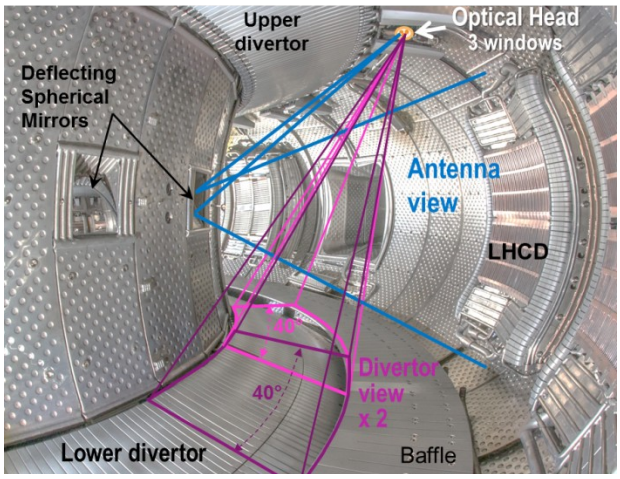

Fig 1: upper port endoscope fields of view (FoV) in WEST

Previously in TS, the endoscopes were located closer to the inner wall, where the upper divertor now takes place. Consequently the endoscopes were moved outward, and a direct view of the antennas was no longer possible since it would have led to a very low angle of incidence. Thus the endoscopes were spun 180° and the antenna is now viewed through a deflecting mirror located in the inner wall. This had a strong impact on the optical design of the antenna view.

2.2 Project constraints

A strong project constraint was to reuse or revamp as much as possible existing parts of the 7 former IR endoscopes which contributed to the success of TS operation for more than 12 years [3]. This challenge concerned only mechanics and optics. All electronic components, i.e. data processing and acquisition system were fully renewed. The foremost requirements and constraints on the design were the following:

- Spatial resolution < 10 mm
- Real Time Monitoring: processing time <100ms
- Wide temperature range up to W melting (3400°C)
- Match with new machine configuration: new endoscopes location, new sight angles
- Withstand heat loads during long pulses, i.e. feature actively cooled plasma facing parts

2.3 Refurbishment and design description

The refurbishment of TS endoscopes lasted 3 years (2016 – 2018), including studies, manufacturing and assembling. Some modifications were required on the mechanics, flanges and bodies, to match new machine interfaces. The most important modifications concern the optics and opto-mechanics (Fig 2). The modifications of the optical design was done with ZEMAX software, at a wavelength of 3.9 microns, similarly to the former one, in order to keep as many lenses as possible unchanged. The new optical parameters are given in Table 1:

Table 1. main optical parameters.

View	FoV	Aperture	Focale length
Divertor	48°	F2.4	9.8 mm
Antenna	9x12° (on mirror)	F3.6	45.7 mm (w/o mirror)

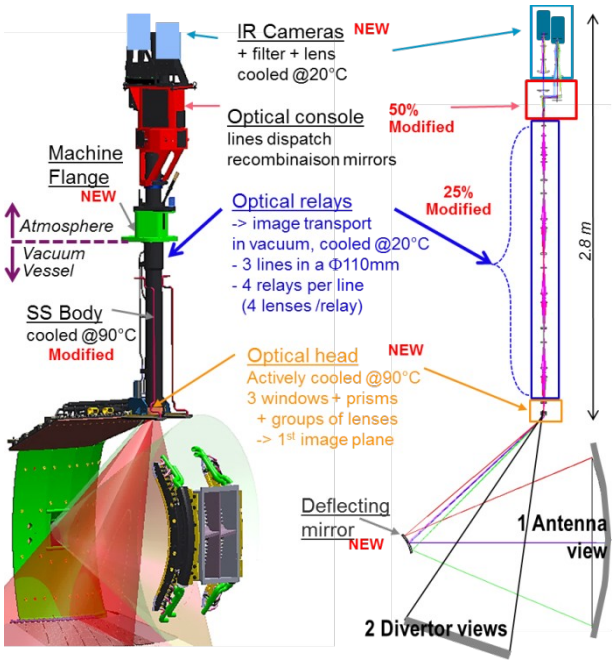

Fig 2: Upper endoscopes for antennas and divertor views. Left = engineering view, right=optics principle

From bottom to top, the modifications concern:

Deflecting mirrors

The deflecting mirror is a new component imposed by the endoscope relocation. It is a 170x170 mm bulk molybdenum part, uncoated, with a convex spherical surface (radius of curvature = 250 mm). It was polished by conventional methods, with a roughness of ≈10 nm, and spherical defect <100nm RMS.

author's email: xavier.courtois@cea.fr

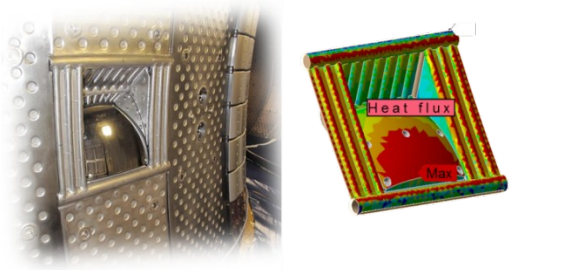

Fig 3: Left: Mirror mounted in the inner wall - Right: heat flux deposition pattern from plasma radiation (max=130 kW/m²)

The advantages of using Mo include a good erosion resistance [4] and a high conductivity ensuring homogeneous temperature and deformation fields. The drawback is a challenging polishing due to the toughness and fragility of the material.The mirror is mounted in a protecting niche, and screwed onto a supporting plate which is cooled by pressurized water flow. The maximum heat flux deposition on its surface for the most radiating plasma scenario (130 kW/m²) leads to a max temperature of 200°C, which is acceptable in terms of surface deformation and parasitic IR radiation.

Optical head

In order to match the new FoVs and sight angles, a new optical head has been designed. A CuCrZr body ensures the protection (Fig 4) to the incoming heat flux. It is cooled by pressurized water at machine temperature by inner channels to withstand up to 1.3kW of plasma radiation. An additional front tube provides a shield against the electrons losses trapped in the magnetic field ripple propagating upward with a zigzag trajectory (up to 3 kW). It is made of Nickel to offer high thermal conductivity and pressure resistance, while remaining easy to manufacture by bending. The 3 windows have a double sapphire disc: the first disc is brazed in a CuCrZr ring which is electron beam welded onto the body, and ensures the tightness. The second disc is held by a screwed washer. It protects the brazed disc in case of pollution, and can be easily replaced or cleaned during maintenance shutdown.

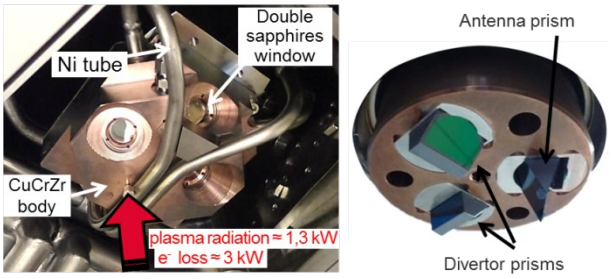

Fig 4: picture of the optical head. Left = the body from inner vacuum vessel, Right = front optics behind the body.

Behind the body is the optical part (Fig 5). It consists first of 3 Silicone prisms which make the deviation of the optical axis. Then a group of lenses makes the first image plane.

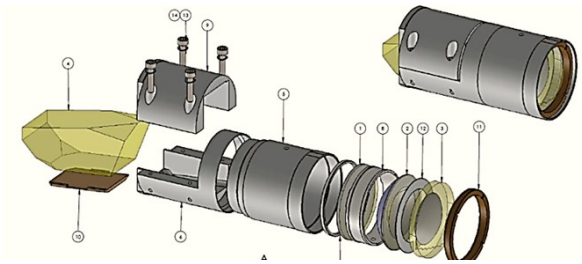

Fig 5: Divertor first optical module: prisms, lenses and mechanical assembling

Optical relays

Each image formed by the optical head is propagated along the optical tube with 4 successive optical relays, 4 lenses per relay. This part is highly constrained by the tube diameter 110mm, which leaves Φ36mm max for the lenses. The optical design effort allowed saving about 80% of the existing lenses, which was valuable given that lenses usually prevail the cost in an optical system. However, the disassembly and reassembly of some unchanged lenses were necessary, due to required modifications of opto-mechanical pieces, but with a low impact on manufacturing costs.

Optical console

The recombination console dispatches the antenna line on the first camera, and gathers the 2 divertor lines on the second camera, thanks to a set of flat gold coated silica mirrors. These mirrors also enable the differential focus adjustments. All the mirrors were degraded and have been replaced identically. However, the mechanical mounting of the mirror was significantly modified to adapt to the new sight angles.

Camera

12 homemade cameras were developed, based on an IR detector from SCD Company. It is an InSb focal plane array which features a 1.5-5.0 µm spectral range, 640x512 pixels per frame with acquisition rate of 250 Hz. Around this detector, we have designed manufactured and assembled the camera with a soft iron magnetic shield tested up to 140 mT, a water cooled casing, and rugged power supply and embedded electronic boards (Fig 6). The inner band-pass filter is thermalized by a Peltier module in order to suppress the offset variation due to the filter background radiation.

The camera is fully controlled by an external FPGA board which ensures the communication with the detector, the data acquisition and real time processing with following frame rates capabilities:

- 150 Hz with 1 adaptive Integration Time (IT)
- 50 Hz with 4 IT or 33Hz with 6 IT to allow a very high dynamic range.
- 1500 Hz with 1 IT with tight windowing

author's email: xavier.courtois@cea.fr

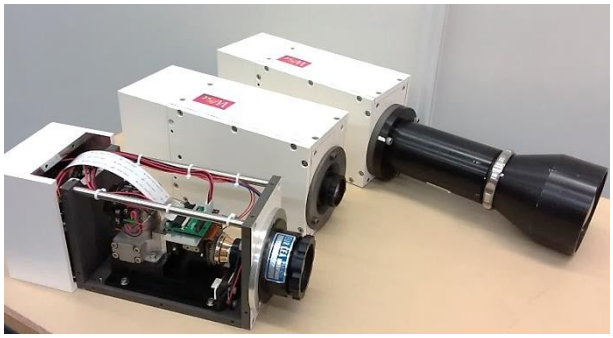

Fig 6: Home-made cameras fitted with various lenses

The FPGA board also performs in real time the bad pixels replacement, the correction of non-uniformity of the detector, the digital level to temperature conversion (cf. §4), and the extraction of the maximum temperature in the predefined Region Of Interest (ROI) of the monitored components surface.

3 Hardware architecture and data handling

The new hardware architecture is composed of 5 identical Acquisition Units (AU) (Fig 7). An AU consists of a PXI crate containing 3 FPGA boards, and a Linux PC (CentOS distribution) for the data acquisition and temporary storage. At the end of pulse, the data are uploaded in the database for display and post processing.

The FPGA board is the heart of the protection system. It communicates the results of temperature real time calculation to the Plasma Control System (PCS) on 2 independent outputs: (i) Each ROI max temperature is sent via a fast network, toward the PCS, to reduce and control the injected power when the temperature approaches the temperature threshold [5]. (ii) In case of overheating, a flag is sent on a hard output to the interlock system which causes a soft plasma landing.

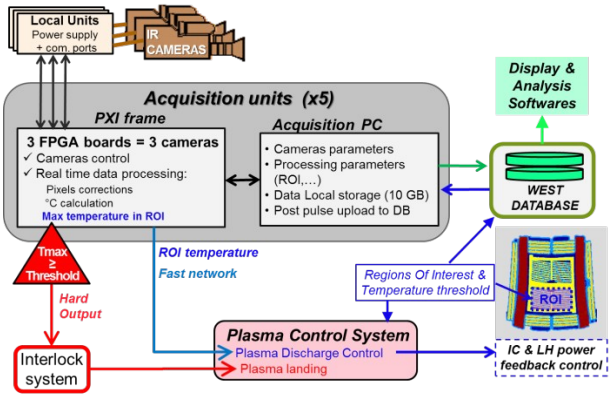

Fig 7: hardware architecture and data handling

4 Temperature calculation and monitoring

4.1 Principle

The temperature calculation procedure is similar to that used for TS [6], with the mirror as new component. It is performed in real time by the FPGA. It takes into account the laboratory camera calibration, and the transmission loss of all the optical lines. In that aim, the optical system is divided in 3 independent parts, which are considered at different temperature: the mirror (for antenna view) @90°C, the optical head window @90°C, and the optical relays and console @ 20°C. The camera lens and the filter are taken into account in the camera calibration. Before conversion to temperature, the calculation is performed in luminance. For each above mentioned optical part, starting by the top of the system, the parasitic signal radiated by the optical part at its given temperature is subtracted to the luminance signal measured by the camera, and the transmission loss is applied (i.e. the signal is divided by the transmission coefficient). The next optical part is then calculated. The parasitic reflections are considered as negligible since all the lenses are antireflection coated. At the end, the estimated radiation luminance on the component is obtained and converted in temperature using the camera calibration curves.

Thanks to this method, cameras or optical relay tubes can be replaced or switched without recalibration of the full optical line since the calculation takes into account these parts individually.

4.2 Temperature monitoring

It is obvious that emissivity is a key parameter in IR temperature measurement. This parameter is an endless issue since emissivity may vary with temperature, surface roughness, material ageing and incidence angle. As a consequence, regarding real time machine protection, the temperature considered is always the luminance temperature, i.e. with emissivity=1. The temperature threshold applied in each ROI of the monitored components integrates the emissivity of the material. For a safe monitoring, the emissivity chosen to minimize the luminance temperature threshold at the maximum acceptable temperature for the material, is the lowest known emissivity. This emissivity is initially determined either from bibliography, material test bed or experience, and can be modified cautiously during plasma campaign according to observed phenomena and modelling.

For post analysis, any emissivity ≤1 can be applied on the IR data. Pre and post pulse analysis tools and detailed simulations are developed in parallel to better analyse and understand the impact of variable emissivity and reflections on measured temperature [7] [8].

5 Laboratory characterization

5.1 Calibrations and optical transmissions

All calibrations and optical transmissions are measured in laboratory for each endoscope, using black bodies featuring reference temperatures up to 1600°C. Extrapolations are performed for higher temperatures thanks to a good linearity of the detector. The same procedures as the ones used for TS diagnostic [9] are applied. A dedicated test bed reproduces the machine

author's email: xavier.courtois@cea.fr

configuration with divertor and antenna mock-ups and serves to tune the focus, adjust the mirrors for the correct recombination of the 2 divertor lines (see §2.3).

The total measured transmission coefficient in the field centre was measured at about 0.4 for the divertor view, and 0.3 for the antenna view.

5.2 Optical performances

The optical performances can be expressed in different ways which are given here after. The optical performances are summarised in Table 2.

Pixel resolution:

The pixel resolution is the projection of a pixel size in the object plane. It varies significantly for the divertor, due to the inclination of the line of sight from 2.3 to 5.6 mm/pixel. For antennas, values rank from 3.9 to 4.4 mm/pixel.

Imaging spatial resolution:

The modulation transfer function (MTF) is a conventional method to characterize the response of an optical system, and gives the imaging spatial resolution.

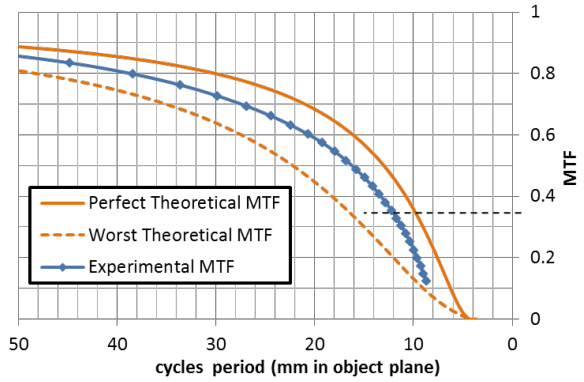

Fig 8: Antenna view MTF - Horizontal slit.
A cycle is a black / white line alternation

The measured MTF is compared to the theoretical MTF which is the product of the optical MTF computed by ZEMAX and the MTF of pixel size. The measured MTF (Fig 8) is between the perfect case (all the lenses are perfectly machined and mounted) and the worst commonly expected case (case for which the probability to have a bad combination of the tolerances, within those allocated for manufacturing and mounting, is less than 10%), which is a satisfying result. The lowest acceptable imaging resolution is commonly done for 35% MTF, given in Table 2.

Quantitative spatial resolution:

The MTF is inadequate to qualify thermal measurement performances; thus the Slit Response Function (SRF) was measured to quantify thermal spatial resolution (Fig 9). This method allows determining the correction to be applied to the measurement of small objects which are spatially under-resolved. This is the case for example for the gaps between divertor targets, or thin plates between LHCD antenna wave guides.

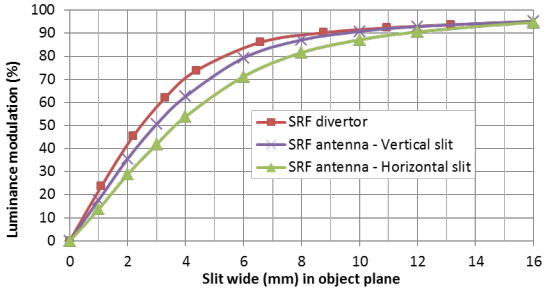

Fig 9: Slit Response Function: luminance of a variable width slit which is illuminated from behind.

For the divertor view, the horizontal and vertical directions (regarding the image aspect) are equal, which is not the case for the antenna view due to the deflecting mirror inclination. The SRF is given in Table 1 for 80% of luminance modulation which corresponds to a measurement error of 10% @1000°C, for wavelength of 3.9 µm. This result is consistent with the theoretical SRF extracted from ZEMAX with an accuracy of less than 10% for antenna view, and ≈40% for divertor view. The latter is probably the result of a defocus due to an imperfect adjustment of console mirrors.

Table 2. Optical performances measured in lab.
Note: vertical slit give horizontal resolution, and reciprocally.

Resolution (mm)	Pixel projection *	MTF 35%	SRF 80%
Divertor Vert.	2.7	9.4	5.4
Antenna Vert.	4.3	12.0	7.6
Antenna Horiz.	3.9	10.4	6.1

* at MTF and SRF measurement location on Fig 10 and 11

These results are in line with the project requirements.

Minimum measurable temperature:

The minimum measurable level is determined for a level significantly higher than the background noise, typically 100 Digital Level. This level is approximately 150°C for the divertor view and 200°C for the antenna view. Images can be observed under these thresholds, but the temperature measurement is not reliable.

6 Plasma operation and first results

The system was under operation early 2018, with 2 endoscopes providing 2 antenna views and 4 divertor views; it is planned to be fully installed mid-2019. The figure Fig 10 shows 2 divertor views recombined on one detector. One can observe the differential heat flux of the 2 strike points. The period corresponding to WEST magnetic field ripple (1 toroidal coil per 20° [10]) is clearly visible.

author's email: xavier.courtois@cea.fr

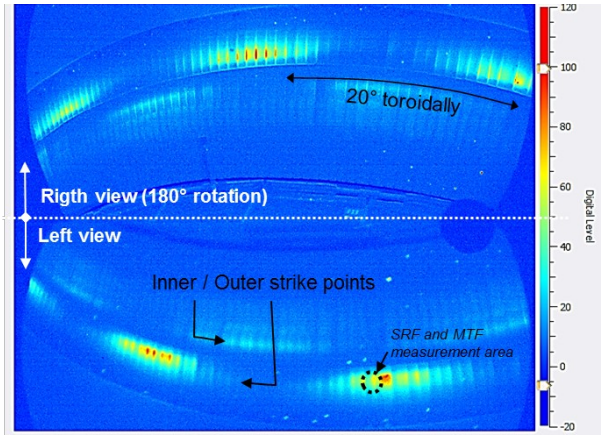

Fig 10: Port 6 divertor IR image during pulse #53223 (LH+IC power = 2+0,6 MW Ip=500 kW). Color scale is the luminance in arbitrary unit.

The figure Fig 11 presents an IR image of an ICRH antenna during a disruption with a wide spectrum plasma radiation contributing to reflections on all the metallic surfaces.

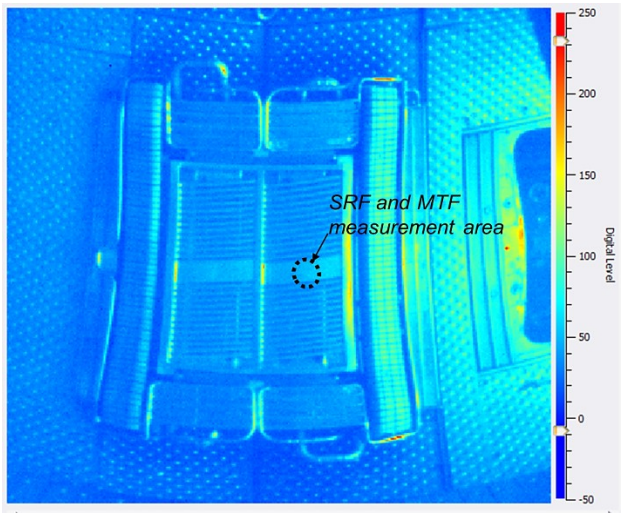

Fig 11: Port 2 ICRH antenna IR image during pulse #53132 on plasma disruption. Color scale is in arbitrary unit.

7 Conclusion

The IR system for WEST is a set of diagnostics dedicated to PFCs protection and machine operation, but it is also an essential support to physics investigations.

Seven endoscopes located in upper ports viewing the whole lower divertor and the 5 heating devices have been upgraded and manufactured. Their optical performances are in line with project and design requirements. The endoscopes are progressively installed on WEST. The total renewing of the cameras and of the data processing and acquisition system is achieved and gives satisfying results in operation.

Some upgrades are foreseen:

- Manufacturing new camera lenses for divertor view to enhance the resolution
- Developpment of an embedded black body on WEST articulated inspection arm for in-situ calibration under vacuum and temperature conditions.
- Improvement of temperature calculation by measuring automatically the first optics temperature duirng pulses.
- Development of an inovative machine protection software to optimise the safe operationnal domaine.

author's email: xavier.courtois@cea.fr

Acknowledgments

This work has been carried out within the framework of the EUROfusion Consortium and has received funding from the Euratom research and training programme 2014-2018 under grant agreement No 633053. The views and opinions expressed herein do not necessarily reflect those of the European Commission.

References

[1] J. Bucalossi, et al. Fusion Eng. Des. **89** (2014) 907–912.
[2] X. Courtois, et al. Fusion Eng. Des. In Press, doi 10.1016/j.fusengdes.2018.05.042
[3] D. Guilhem, et al. Fusion Eng. Des. **74** (2005) 879–883.
[4] B. Eren, et al. Journal of Nuclear Materials **438** SUPPL (2013), S852-S855
[5] P. Moreau, et al. Fusion Eng. Des. **82** (2007) 1030-1035
[6] D. Guilhem, et al. QIRT J. 2. (2005) 77-96.
[7] MH. Aumeunier, et al. Review of Scientific Instruments **81**, 10E524 (2010)
[8] MH. Aumeunier, et al. Nuclear Materials and Energy, 12, (2017) 1265-1269
[9] C. Desgranges, et al. Nuclear. Ints. & Methods in Physics Research, A **879** (2018) 121-133
[10] R. Mitteau, et al. Fusion Science and Technology, 56:3, (2009) 1353-1365